Mesosphere-Lower-Thermosphere Neutral Density Measurements from Low-cost COTS Accelerometers and Ionization Gauge

Nathan Graves[1] (gravesn@my.erau.edu) Aroh Barjatya[1] Rob Clayton[1] Henry Valentine[1] Gerald Lehmacher[2]

(1) *Embry-Riddle Aeronautical University, Daytona Beach, FL, United States*, (2) *Clemson University, Clemson, SC, United States*

Abstract

Measurements of aerodynamic drag on objects can be used to determine the density of the medium. The Space and Atmospheric Instrumentation Laboratory at Embry-Riddle Aeronautical University launched a midlatitude sounding rocket named SpEED Demon from Wallops Flight Facility in August 2022. SpEED Demon has a comprehensive suite of instruments for electrodynamics and neutral dynamics measurements. Among these are sensitive low-cost MEMS accelerometers allowing for neutral density measurements up to 100km in altitude. In addition to sensitive accelerometers on the main payload, four ejectable subpayloads also carry an accelerometer providing simultaneous multi-point neutral density measurements, akin to a 'falling cylinder' experiment. The measurements of neutral density via accelerometers will be cross-validated by an ionization gauge onboard the main payload. We present the flight performance and results of this measurement technique from the SpEED Demon launch.

Drag-based Density Measurement Background

Measurements of neutral density in the altitude range of (50-200km) have been a target of sounding rocket missions for a long time. Neutral density measurements have been gathered via the active and passive falling sphere [1][2], neutral mass spectrometers [3], and more recently hot and cold cathode ionization gauges [4].

A recent rocket payload carried a MEMS accelerometer, showing good agreement with an ionization gauge instrument on the same payload up to 80km altitude [5]. MEMS accelerometers continue to improve in cost, size, and sensitivity. Additionally, they require no external interfacing making them easy to integrate into any rocket mission. Extracting neutral density information from accelerometer measurements is therefore worthwhile.

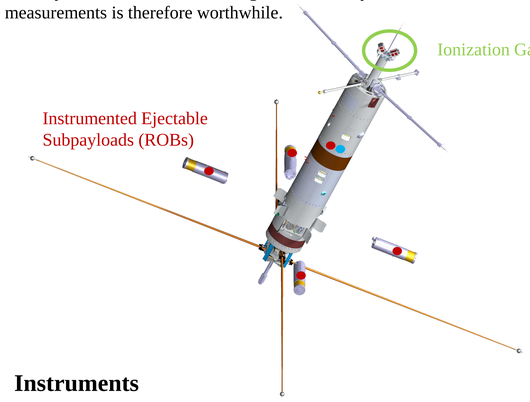

Instruments

Cold Cathode Ionization Gauge [6]
- Pfeiffer PKR360 x 2
  - Mounted 45° from axial fore end on the main payload
  - Measurement range: 7.5e-10 to 750 torr
  - 5kHz measurement frequency
  - 5% Repeatability
  - Calibrated at Clemson University

ADXL 355 [7]
- 1x Centrally located on main payload, 4x on subpayloads
- ±2g measurement range
- ~30 µg resolution
- 0.25 - 2.5 kHz measurement frequency

Kionix KXR94-2283 [6]
- 1x Centrally located on main payload
- ±0.5g measurement range
- 5kHz measurement frequency
- Flight Heritage: MTeX[5]

PKR360 Ionization Gauge Sensor

Table 1: Mechanical specifications of the payloads relevant to drag effects on the accelerometers.

Parameter	Main Payload	Subpayload
Acceleration Noise [µg/sqrt(Hz)]	45/25	25
Payload Length [mm]	2200	335
Payload Diameter [mm]	450	84
Ballistic Coefficient [kg/m^2]	85-550	40-190
Sampling Rate [kHz]	5/2.5	250

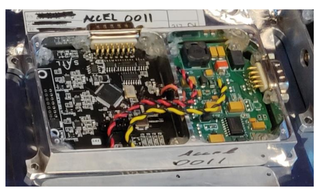

Main Payload Accelerometer Box

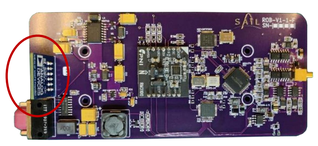

Subpayload PCB

Ionization Gauge Calibration

Figure 1: Image of the calibration setup in SAIL. Test Equity 115A shown on right. Left: Up to 3 Keithley 2450 sourcemeters for simultaneous calibration.

Ionization Gauge Flight Data

Figure 2 shows the calibrated pressure data from each of the ionization gauges on the main payload. The data are compared against the NRL-MSISE00 model. Due to the ionization gauge being mounted on the nose of the payload that may be moving in the ram direction at supersonic velocities, they will measure an elevated pressure from the background. This can be corrected for by computing a ram factor [5][9] according to the following equations :

$$RF(S) = \sqrt{\frac{T_1}{T_2}}\exp(-S^2) + \sqrt{\pi}\,S\,(1+\mathrm{erf}(S))\ (1)$$

$$S = \frac{v\cos(\alpha)}{\sqrt{2kT_1/m}}\ (2)$$

Where α is the angle of attack to the ram direction, T_1 is the neutral temperature, T_2 is the temperature within the gauge, and $\bar{m}$ is the mean molecular mass.

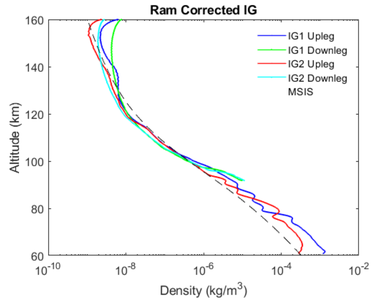

Figure 3: Ram-corrected ionization gauge density data.

Accelerometer Flight Data

$$a_{drag} = C_d\frac{\rho\,v^2}{2m}A_{proj}\ (3);\quad \rho = \frac{2m\,a_{drag}}{C_d\,A_{proj}\,v^2}\ (4)$$

Figure 4 shows the theoretical acceleration due to drag for the subpayload experiment as a function of altitude and relative velocity between the object and the medium. It is assumed that the projected area to ram and drag coefficient is constant. The nominal rocket flight path is shown. The analog and digital accelerometers flown should be capable of resolving density up to 105-110 km, in the best case. More expensive accelerometers are also shown, as future instruments of interest. The Seismic MEMS devices have been designed into the next iteration of the instrument.

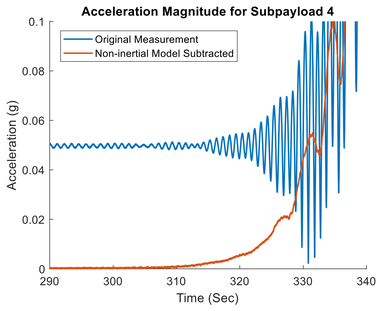

Figure 5: A comparison of raw subpayload acceleration magnitude data and the resulting signal after non-inertial accelerations are removed. Remaining variation is due to dynamic projected area and drag coefficient effects.

The ionization gauges were calibrated in a two-step process. The voltage output of the PKR360 sensor was calibrated against an MKS Baratron® high accuracy gauge at Clemson University. Three runs were performed for each gauge, involving testing a range of pressures over the expected flight conditions. An additional calibration of the voltage measurement box was performed in the Space and Atmospheric Instrumentation Lab at Embry-Riddle Aeronautical University. Calibrating its counts to voltage conversion over a temperature range of 25°C to 55°C in 10°C steps. The pressure calibration fit is +/- 20% over the range to 10^{-5} Torr.

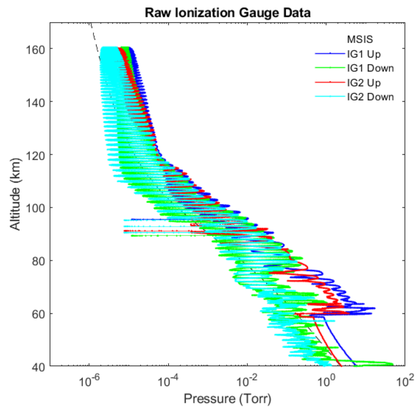

Figure 2: Calibrated Ionization Gauge pressure from both gauges on the upleg and downleg of the flight.

Figure 3 shows the result of applying the ram factor to the ionization gauge data and averaging over the spin period. As the attitude solution is still being refined, the exact angle to the ram direction may be slightly off, resulting in a modulation at the spin frequency. This effect can also be caused by winds shifting the ram direction angle, so when the attitude solution is refined, wind measurements can potentially be made. Below 80km on the downleg the payload reentered the atmosphere and began tumbling. This results in highly turbulent motion that distorts the ram correction factor. Notably in the uncorrected plot this is shown by downleg data being much closer to the model in the range of 60-80km, the ram factor has shifted and will need more considerations to account for its effects.

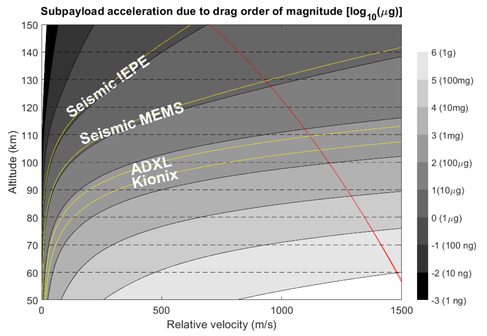

Figure 4: Theoretical acceleration due to drag for subpayloads compared to sensor noise floors. Nominal rocket altitude-velocity trajectory shown in red.

In order to solve for density in Equation (4), we need to have a measurement of the acceleration due to drag, however, unless the accelerometer is positioned precisely at the center of mass, non-inertial accelerations will also be present due to the rotating reference frame of the accelerometer. These non-inertial accelerations will institute an artificial noise floor unless they are subtracted out as shown in Figure 5.

$$\boldsymbol{a}_{fict} = \underbrace{\dot{\boldsymbol{\omega}}\times\boldsymbol{r}}_{\text{Euler}} + \underbrace{\boldsymbol{\omega}\times\boldsymbol{\omega}\times\boldsymbol{r}}_{\text{Centrifugal}} + \underbrace{2\boldsymbol{\omega}\times\dot{\boldsymbol{r}}}_{\text{Coriolis}}\ (5)[11]$$

Equation (5) describes the non-inertial (fictitious) accelerations present due to the rotating reference frame of the accelerometer.

ω is the angular velocity vector of the rotating frame, and **r** is the position vector of the accelerometer in the center of mass frame. Since the accelerometer is fixed in the center of mass frame, the Coriolis term will vanish, but the Euler and Centrifugal terms are included in the model. The angular rates are given by an IMU onboard each subpayload.

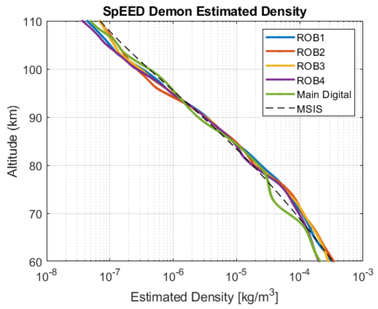

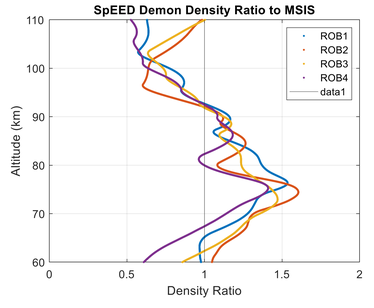

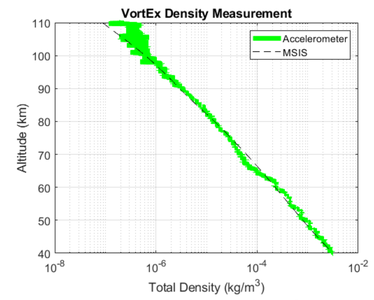

Figure 6: Estimated density data from two sounding rocket flights, SpEED Demon and VortEx. Compared to model background NRL-MSISE00. ROB is Subpayload, and MP is the main payload. The VortEx flight did not deploy subpayloads and only has a main payload measurement.

Estimated density, as shown in Figure 5, is computed using Equation (4). The acceleration due to drag (a_{drag}) is the sensor measurement after the non-inertial model has been subtracted. The velocity is derived from GPS measurements. The projected area (A_{proj}) is assumed to be the area of the payloads with the long axis oriented perpendicular to the ram direction (length multiplied by diameter in Table 1). Since the payloads are coning, this is a poor assumption, and the raw acceleration magnitude measurements vary sinusoidally with this changing area. However, computing the signal envelope of the acceleration signal will result in a value close to this maximum area. The drag coefficient (C_d) is applied using published data on circular cylinders in a Reynolds number range of 10-10^6 [10]. For altitudes above ~80km, transitional flow conditions begin, and free molecular flow modeling should be applied. This is one cause of underestimates in the high-altitude data.

Improvements

The largest assumption in the current technique is the projected area in the ram direction remains constant. The projected area for the subpayloads remains within +/-5% for a 30° deviation from the assumed case, however it drops off quickly for larger deviations. By processing gyro and magnetometer data with an extended kalman filter, estimates of the subpayload attitude throughout the flight can be produced. Current attitude solutions (Example in Figure 7) show that the subpayloads did not frequently (or ever for some) exceed a 30° deviation from the assumed case, but they do not account for variations seen in the data.

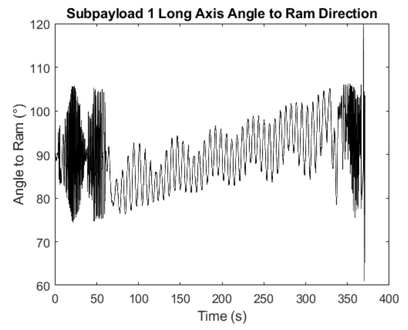

Figure 7: Current attitude solution for subpayload 1

Takeaways

- The flight performance of a distributed set of accelerometers measuring neutral density drag has been demonstrated up to an altitude of 110km. This demonstrates that the 'falling cylinder' technique can be applied in a similar manner as prior 'falling sphere' experiments.
- Refinement and application of an attitude solution to subpayloads may allow for extending this measurement slightly to 115km for all subpayloads and determination of zonal and meridional winds >20m/s up to an altitude of 60km.
- Using more sensitive, larger, and expensive accelerometers can increase density/wind measurement altitude up to ~150km/110km. These have been integrated into the next version of the subpayload and will be deployed in October.
- Direct Simulation Monte-Carlo (DSMC) free molecular flow simulations will be conducted to verify the ionization gauge ram factor on the main payload and acquire a more accurate drag coefficient value for the subpayload at higher altitudes and varying angles of attack.

References

[1] Philbrick, C. R., A. C. Faire, D. H. Fryklund, Measurement of atmospheric density at Kwajalein Atoll, 18 May 1977, *Rep. AFGL TR 78-0058*, 113pp. Air Force Geophys. Lab., 1978 [NTIS AD#054784]

[2] Schmidlin, F.J., Lee, H.S., Michel, W., 1991. The inflatable sphere: A technique for the accurate measurement of middle atmosphere temperatures. J. Geophys. Res. 96 (D12), 22673–22682.

[3] Offermann, D., 1974. Composition variations in the lower thermosphere. Journal of Geo Research 79, 4281-4293.

[4] Lehmacher G.A., Gaulden T.M. Larsen M.F., Craven J.D., Multiple neutral density measurements in the lower thermosphere with cold-cathode ionization gauges, Journal of Atmospheric and Solar-Terrestrial Physics, Volume 92, 2013, Pages 137-144, ISSN 1364-6826, https://doi.org/10.1016/j.jastp.2012.11.002.

[5] Lehmacher, G., *et. al.*, On the Short-term Variability of Turbulence and Temperature in the Winter Mesosphere. *Annales Geophysicae* **36,** 4 (2018). DOI: 10.5194/angeo-36-1099-2018

[6] Pfeiffer Vacuum, https://www.pfeiffer-vacuum.com/en/

[7] Kionix, https://www.kionix.com/

[8] Analog Devices, https://www.analog.com/en/products/adxl355.html

[9] Patterson, G.N., 1956. Molecular Flow of Gases. John Wiley and Sons, New York.

[10] Heddleson, C. F., et al., 1957. Summary of Drag Coefficients of Various Shaped Cylinders. DTIC ADA395503

[11] Thornton, S. T., & Marion, J. B. (2003). Classical dynamics of particles and systems (5th ed.). Brooks/Cole.